International Journal of Heat and Mass Transfer 52 (2009) 1193–1205

Contents lists available at ScienceDirect

International Journal of Heat and Mass Transfer

journal homepage: www.elsevier.com/locate/ijhmt

Entropy generation due to natural convection in non-uniformly heated porous isosceles triangular enclosures at different positions

Yasin Varol [a,*], Hakan F. Oztop [b], Ioan Pop [c]

[a] Department of Mechanical Education, Firat University, 23119 Elazig, Turkey
[b] Department of Mechanical Engineering, Firat University, 23119 Elazig, Turkey
[c] Faculty of Mathematics, University of Cluj, CP 253, 3400 Cluj, Romania

ARTICLE INFO

Article history:
Received 1 July 2008
Received in revised form 22 August 2008
Available online 10 November 2008

Keywords:
Entropy generation
Porous medium
Natural convection
Isosceles triangular
Non-isothermal temperature profile
Numerical results

ABSTRACT

Entropy generation due to natural convection in isosceles triangular enclosures with inclination angles (φ) filled with a fluid-saturated porous medium has been studied numerically. The enclosure has different inclination angles and it is non-uniformly heated from one side. The finite difference technique was adopted to solve the governing equations of this natural convection problem. Then, entropy generation due to heat transfer irreversibility (HTI) and fluid friction irreversibility (FFI) was calculated from its definition using dependent variables of velocities and temperature fields. Calculations were performed for different Rayleigh numbers Ra in the range of $100 \leqslant Ra \leqslant 1000$ and inclination angle, $0^\circ \leqslant \varphi \leqslant 180^\circ$. It is found that both inclination angles and Rayleigh numbers make important effect on natural convection heat transfer, fluid flow and entropy generation. The highest entropy generation due to HTI and FFI and stream function are observed at $\varphi = 90^\circ$. Multiple cells were formed at this angle. Streamlines, isotherms and entropy contours are symmetric inside the enclosure for both $\varphi = 0^\circ$ and $\varphi = 180^\circ$.

1. Introduction

Porous layers have been studied extensively in last years due to its wide applications in geothermal systems as reviewed by Cheng [1] and Bejan [2]. Based on their paper, these kinds of applications can be found for geothermal energy extraction, grain storage, thermal insulation, etc. Wide application can be found in several books on porous media Nield and Bejan [3], Ingham et al. [4], Ingham and Pop [5], Vafai [6] and Vadasz [7]. Bejan and Poulikakos [8] proposed the using of porous material inside the attic space to decrease the heat transfer.

Many researchers have studied the natural convection heat transfer and fluid flow in triangular shaped enclosures filled with viscous fluid due to its important applications as attics, roofs, electronic equipments or different shaped building materials. Natural convection analysis in such geometries has been performed by Akinsete and Coleman [9], Asan and Namli [10,11], Ridouane et al. [12], Holtzman et al. [13], for isothermal and Basak et al. [14,15] for non-isothermal boundary conditions. All of these studies indicate that both aspect ratio of triangular enclosure and Rayleigh number affects the heat transfer and flow fields.

The number of studies on natural convection in triangular enclosures filled with fluid-saturated porous media is very limited. Basak et al. [14] made recently a numerical study solving the Navier–Stokes and energy balance equations for a triangular enclosure filled with a porous medium using a penalty finite element analysis with bi-quadratic elements. They analyzed two cases based on temperature boundary conditions as case I: two inclined walls are uniformly heated while the bottom wall is isothermally cooled and case II: two inclined walls are non-uniformly heated while the bottom wall is isothermally cooled. They found that the local Nusselt numbers for the bottom wall are maximum at the bottom corner points for uniform heating. On the other hand the local Nusselt number shows little variations due to non-uniform heating especially for the Darcy number Da in the limit $Da \leqslant 10^{-4}$. Varol et al. [16–18] have performed studies on natural convection in porous right-angle triangular enclosures by adding some solid objects to control heat transfer. Further, Basak et al. [19,20] investigated the natural convection in triangular enclosures filled with porous media.

The wide theory on entropy generation is given by Bejan [21,22]. Entropy generation in systems in which natural convection occurs is an important issue in engineering applications because it gives information about local and global losses of energy due to heat transfer and fluid friction irreversibility. Thus, the energy saving can be obtained by reducing these losses. The subject is mostly analyzed for rectangular, square or circle shaped porous enclosures in the literature. Baytas [23] and Zahmatkesh [24] investigated the entropy generation for inclined square and horizontal square enclosures, respectively. They observed that en-

* Corresponding author. Tel.: +90 424 237 0000x4219; fax: +90 424 236 7064.
E-mail address: ysnvarol@gmail.com (Y. Varol).

0017-9310/$ - see front matter © 2008 Elsevier Ltd. All rights reserved.
doi:10.1016/j.ijheatmasstransfer.2008.08.026

Nomenclature

Be	Bejan number
g	gravitational acceleration, $m\,s^{-2}$
k	thermal conductivity of the fluid, $W\,m^{-1}\,K^{-1}$
K	permeability of the porous medium, m^2
L	length of the triangle, m
n	normal direction on a plane, m
N	dimensionless entropy generation number
Nu	local Nusselt number, $Nu = (-\partial\theta/\partial n)_{\text{hot wall}}$
Ra	Darcy-modified Rayleigh number, $Ra = (g\beta K(T_H - T_C)L)/\upsilon\alpha_a$
S'''_{gen}	entropy generation rate per unit volume, $W\,m^{-3}\,K^{-1}$
T	fluid temperature, K
T_0	$(T_H + T_C)/2$, K
u, v	velocity components along *x*- and *y*-axes, respectively, $m\,s^{-1}$
U,V	non-dimensional velocity components along *x*- and *y*-axes, respectively, $(uL/\alpha_a, vL/\alpha_a)$
x,y	dimensional Cartesian coordinates, m
X, Y	non-dimensional coordinates, $(X = x/L, Y = y/L)$
ΔT	temperature difference $(T_H - T_C)$, K
Greek letters	
α_a	thermal diffusivity of porous media, $m^2.s^{-1}$
β	thermal expansion coefficient, K^{-1}
λ	amplitude of the sinusoidal function
φ	inclination angle, deg
θ	non-dimensional temperature, $\theta = (T - T_C)/(T_H - T_C)$
μ	dynamic viscosity $(kg\,m^{-1}\,s^{-1})$
ϕ	irreversibility distribution ratio
υ	kinematic viscosity, $m^2.s^{-1}$
ψ	dimensional stream function, $m^2.s^{-1}$
Ψ	non-dimensional stream function, $\Psi = \psi/\alpha_a$
Subscript	
C	cold
H	hot
max	maximum
min	minimum

ergy losses can be reduced with increasing Rayleigh number and inclination angle. It should be mentioned to this end that the only study on entropy generation in a partially heated isosceles triangular enclosure filled with a clear-fluid (Newtonain fluid) was performed by Varol et al. [25].

Non-isothermal thermal boundary conditions for studies of natural convection in enclosures filled with clear and porous fluids were used by several authors. Sarris et al. [26], Bilgen and Ben-Yedder [27] applied the non-isothermal boundary condition for a square enclosure filled with a clear-fluid, while Saeid [28] and Varol et al. [29] applied these thermal conditions for porous square enclosure.

The main originality of the present work is the application of non-isothermal boundary condition onto a boundary of inclined isosceles triangular enclosures filled with porous media and its second law analysis due to natural convection. The above literature survey clearly shows that there is no study in the literature on entropy generation analysis in non-isothermally heated and inclined isosceles enclosures.

2. Problem formulation

The general schematic configuration is a two-dimensional inclined isosceles triangular enclosure filled with a porous medium as shown in Fig. 1(a) along with the coordinates and boundary conditions. Non-isothermal boundary conditions were applied to the long side of the isosceles triangular enclosure and other two boundaries are adiabatic. The governing equations for the steady-state, two-dimensional, incompressible flow with the Darcy–Boussinesq approximation and constant fluid properties can be written in dimensionless form as follows:

$$\frac{\partial^2\Psi}{\partial X^2} + \frac{\partial^2\Psi}{\partial Y^2} = Ra\left(\cos\varphi\frac{\partial\theta}{\partial X} - \sin\varphi\frac{\partial\theta}{\partial Y}\right) \tag{1}$$

$$\frac{\partial\Psi}{\partial Y}\frac{\partial\theta}{\partial X} - \frac{\partial\Psi}{\partial X}\frac{\partial\theta}{\partial Y} = \frac{\partial^2\theta}{\partial X^2} + \frac{\partial^2\theta}{\partial Y^2} \tag{2}$$

where the dimensionless variables are defined as

$$X = \frac{x}{L}, \quad Y = \frac{y}{L}, \quad \Psi = \frac{\psi}{\alpha_a}, \quad U,V = \frac{(u,v)L}{\alpha_a}, \quad \theta = \frac{T - T_C}{T_H - T_C} \tag{3}$$

where Ψ is the stream function which is defined in the usual way as

$$u = \frac{\partial\psi}{\partial y}, \quad v = -\frac{\partial\psi}{\partial x} \tag{4}$$

and *Ra* is the Rayleigh number for a porous medium defined as

$$Ra = \frac{(g\beta K(T_H - T_C)L)}{\upsilon\alpha_a}. \tag{5}$$

The physical meaning of the other variables is given in the Nomenclature. The boundary conditions of Eqs. (1) and (2) as shown in Fig. 1(a) are $\Psi = 0$ for all solid boundaries,

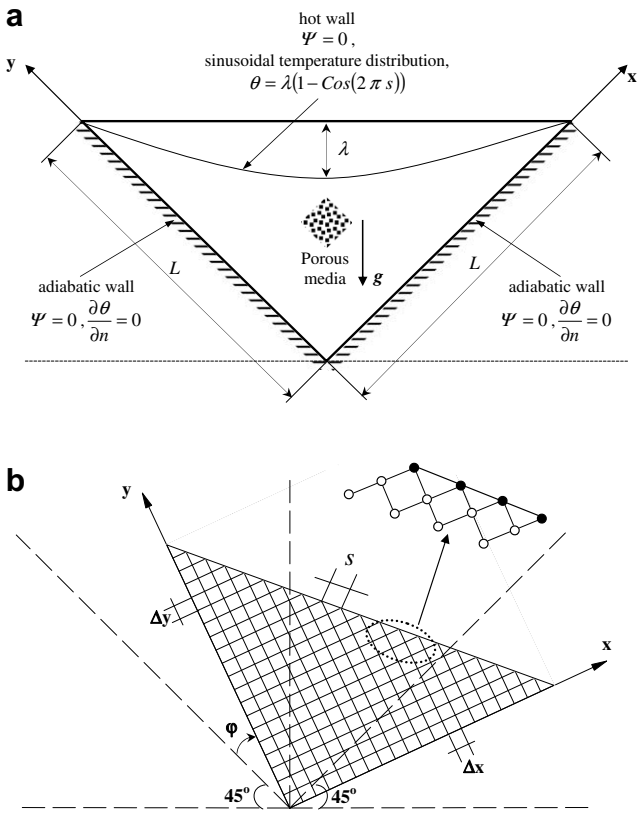

Fig. 1. Physical model: (a) schematical configuration with boundary conditions and coordinates; (b) grid distribution.

$\theta = \lambda(1 - Cos(2\pi s))$ on the top wall and $\frac{\partial\theta}{\partial n} = 0$ on the adiabatic walls, where s is the differential distance on the top wall and n denotes the direction normal to the walls of the cavity. In above boundary condition, the total heat flux q_w is assumed to have the same representation as the case of local thermal equilibrium. In other words, it is assumed that both phases have the same temperature and temperature gradient at the wall as indicated by Alazmi and Vafai [30].

3. Numerical technique

Central difference method was applied for discretization of the governing Eqs. (1) and (2). The solution of linear algebraic equations was performed using Successive Under Relaxation (SUR) method. The iteration procedure terminated under the following condition:

$$\sum_{i,j} |\Phi_{i,j}^{m} - \Phi_{i,j}^{m-1}| \Big/ \sum_{i,j} |\Phi_{i,j}^{m}| \leqslant 10^{-5} \tag{6}$$

where Φ stands for either θ or Ψ, and m denotes the iteration step. The value of 0.1 was used for under-relaxation parameter. The solution domain, therefore, consists of grid points at which equations are applied. Table 1 shows the grid-independency test with iteration number. The execution time for a typical case $\varphi = 0^\circ$, the grid size 61×61, Ra = 1000 for 4173 iterations was around 1 min for a dual core computer. The tests were performed for grids of size from 31×31 to 101×101. Based on obtained results from different grid dimension the 61×61 uniform grid spacing has been used for the present triangular cavity. Grid distribution is also shown in Fig. 1(b). Regular grid distribution is used in this study. The inclined wall was approximated with staircase-like zigzag lines. In other words, rectangular finite difference grid is placed over the triangular enclosure so that the diagonal elements coincide with points on the inclined surface. This is also shown in Fig. 1(b) in detail. Based on the detailed views of boundary grids in Fig. 1, the nodes coincide with boundary of the enclosure.

3.1. Evaluation of heat transfer

Physical quantities of interest in this problem are defined similar to that of Sarris' et al. study [26]. Thus, the local Nusselt number, Nu and the average Nusselt number, Nu_m, which are given by

$$Nu = \left(-\frac{\partial\theta}{\partial n}\right)_{hotwall}, \quad Nu_m = \frac{1}{s}\int_{s=0}^{s=\sqrt{2}} Nu\, ds \tag{7a, b}$$

However, in the present study, the net heat input from the non-isothermal wall into the enclosure is zero, and as a consequence the average Nusselt number is also zero.

4. Entropy generation

The non-equilibrium conditions due to the exchange of energy and momentum, within the fluid-saturated porous medium and at the solid boundaries, cause a continuous entropy generation in the flow field of the porous cavity. This entropy generation is due to the irreversible nature of heat transfer and viscosity effects, within the fluid and at the solid boundaries. From the known temperature and velocity fields, volumetric entropy generation can be calculated by the equation (Baytas [23]),

Table 1
Grid independency test at $\varphi = 0^\circ$ and $Ra = 1000$

Grid dimension (X by Y)	Minimum Nusselt number (Nu_{min})	Maximum Nusselt number (Nu_{max})	Number of iteration
31×31	−2.61	6.85	2311
41×41	−3.25	7.26	3120
61×61	−4.12	7.65	4173
81×81	−4.42	7.83	6720
101×101	−4.27	7.74	9686

Table 2
Comparison of the mean Nusselt number, Nu_m for a square porous cavity with results from the literature at Ra = 1000

References	Mean Nusselt number (Nu_m)	Deviation%
Gross et al. [31]	13.448	0.862
Goyeau et al. [32]	13.470	0.697
Manole and Lage [33]	13.637	0.535
Saeid and Pop [34]	13.726	1.180
Baytas and Pop [35]	14.060	3.527
Present result	13.564	–

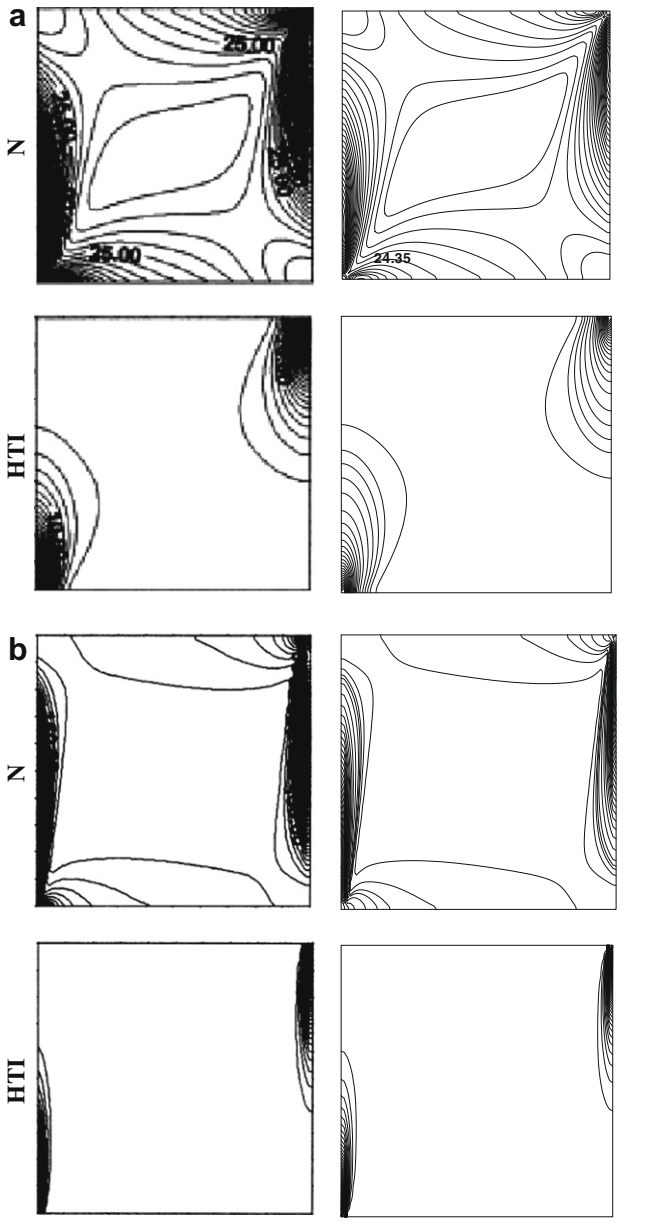

Fig. 2. Comparison of the total entropy generation number (N) and entropy generation φ due to HTI contours obtained with those of Baytas [23] (on the left) and present code (on the right): (a) $Ra = 100$; (b) $Ra = 1000$.

$$S'''_{gen} = \frac{k}{T_0^2}(\nabla T)^2 + \frac{\mu}{KT_0}(u^2+v^2) \tag{8}$$

By using the same dimensionless parameters given in Eq. (3), the dimensionless entropy generation number N is given as

$$N = \left[\left(\frac{\partial\theta}{\partial X}\right)^2 + \left(\frac{\partial\theta}{\partial Y}\right)^2\right] + \phi\left[\left(\frac{\partial\Psi}{\partial Y}\right)^2 + \left(\frac{\partial\Psi}{\partial X}\right)^2\right] \tag{9}$$

In this equation, φ is defined as the irreversibility distribution ratio

$$\phi = \frac{\mu T_0}{k}\left(\frac{\alpha_a^2}{K(\Delta T)^2}\right) \tag{10}$$

and its value is taken equal to 10^{-2} in all calculations. We notice that Eq. (9) consists of two parts. The first part (first square bracketed term at the right-hand side of Eq. (9) is the irreversibility due to finite temperature gradient and generally termed as the heat transfer irreversibility (HTI). The second part (second square bracketed term) is the contribution of fluid friction irreversibility (FFI) to entropy generation. The overall entropy generation, for a particular problem, is an internal competition between HTI and FFI. Usually, free convection problems, at low and moderate Rayleigh numbers, are dominated by the heat transfer irreversibility. Entropy generation number (N) is important for generating entropy generation profiles or maps but fails to give any idea whether fluid friction or heat transfer dominates. The two parameters, namely, the irreversibility distribution ratio (ϕ) and Bejan number (Be)) are achieving an increasing popularity among the researchers of the Second-Law of Thermodynamics. Finally, it is noticed that Bejan number (Be), which is the ratio of heat transfer irreversibility to the entropy production number (N), can be mathematically expressed as

$$Be = \frac{\left[\left(\frac{\partial\theta}{\partial X}\right)^2 + \left(\frac{\partial\theta}{\partial Y}\right)^2\right]}{N} = \frac{HTI}{HTI + FFI} \tag{11}$$

Integration of Eq. (9) over the whole domain to obtain entropy generation number as

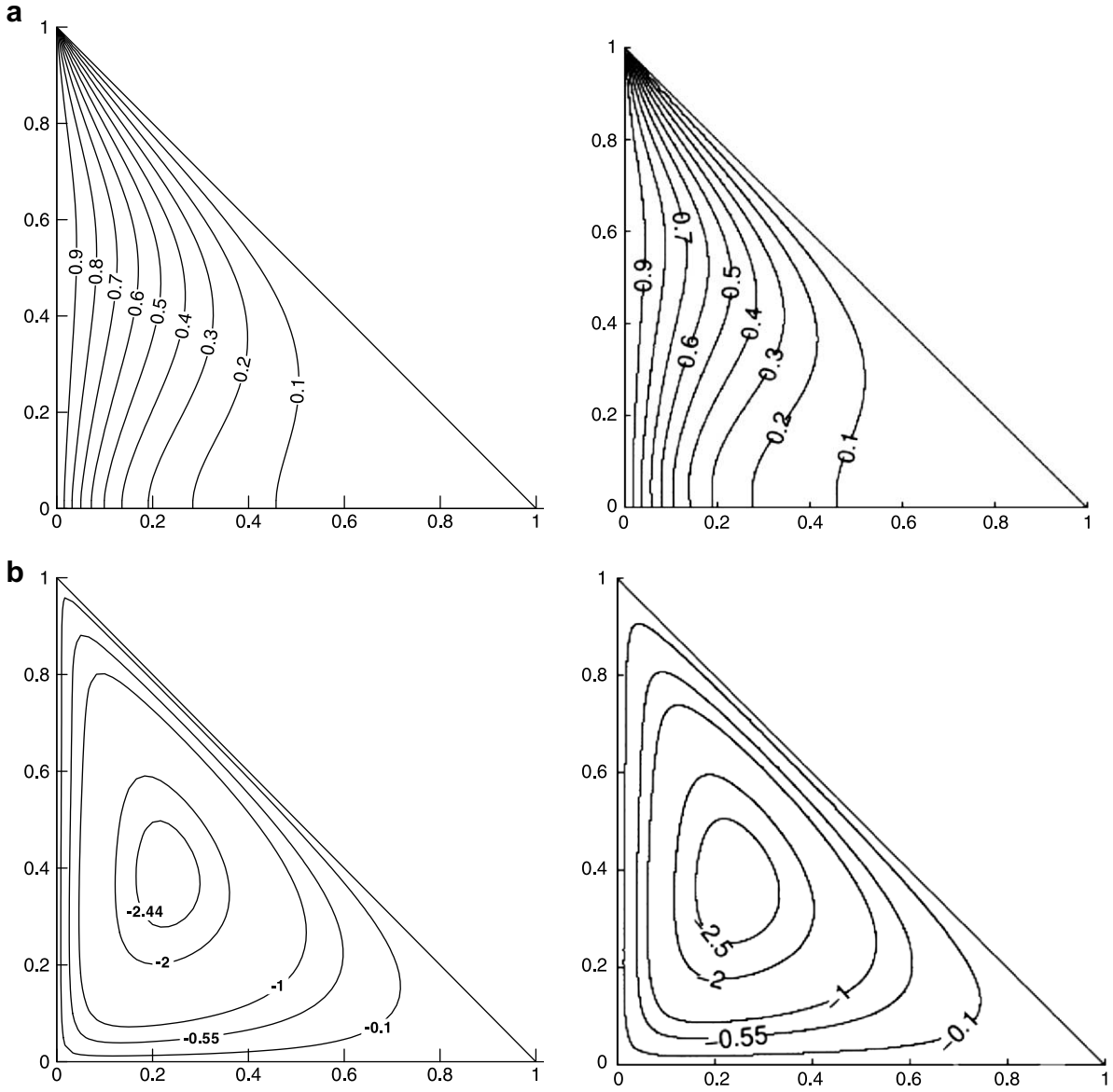

Fig. 3. Comparison of streamlines and isotherms with literature at $Ra = 56$: (a) isotherms for present (on the left) and Basak et al. [19] (on the right); (b) streamlines for present (on the left) and Basak et al. [19] (on the right).

$$N_s = \int_0^1 \int_0^1 N dX dY \tag{12}$$

4.1. Verification of the code runs

Computations were first performed for a widely used benchmark problem of natural convection heat transfer in a differentially heated square porous enclosure for the benchmarking purpose. The obtained numerical results for the mean Nusselt number Nu_m are compared in Table 2 for Ra = 1000 with those given by different authors [31–35]. As it can be seen the obtained result shows good agreement with the results reported by other authors. A maximum difference of 3.527% has been found for Nu_m at Ra = 1000. A second comparison has been also made using the entropy generation results reported by Baytas [23]. Comparison was performed with entropy generation due to heat transfer irreversibility and total entropy generation as shown in Fig. 2(a) (Ra = 100) and Fig. 2(b) (Ra = 1000). As can be seen from this comparison the obtained results show extremely good agreement with those from the open literature. In the third validation test, an acceptable agreement was attained when the contour maps of the isotherms and streamlines of right-angle triangular enclosure, were regenerated for some cases reported by Basak et al. [19], as it is shown in Fig. 3 for Ra = 56.

5. Results and discussion

Second law analysis due to natural convection heat transfer and fluid flow in inclined isosceles triangular enclosures filled with a porous medium has been performed under non-isothermal boundary conditions using a numerical technique for different Rayleigh numbers and inclination angles.

Fig. 4 shows the streamlines (on the left) and isotherms (on the right) for $\varphi = 0^\circ$ at different Rayleigh numbers. The figure shows that flow field is completely symmetric based on the vertical axis

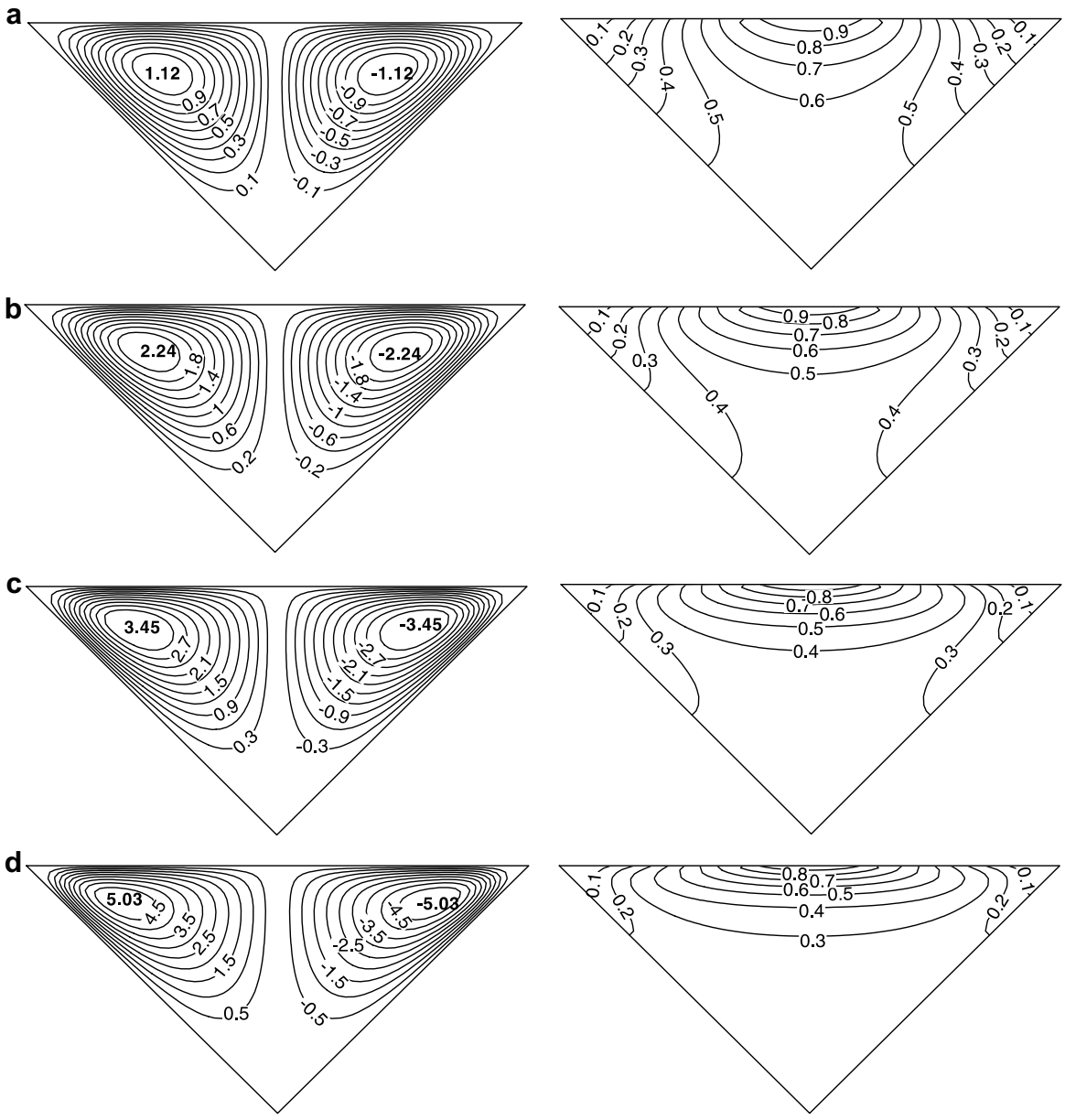

Fig. 4. Streamlines (on the left) and isotherms (on the right) for $\varphi = 0^\circ$: (a) $Ra = 100$; (b) $Ra = 250$; (c) $Ra = 500$; (d) $Ra = 1000$.

and two circulation cells were formed at different rotating direction. Absolute values of stream function are equal to $|\Psi| = 1.12$ for $Ra = 100$. One can guess the direction of rotating flow using the definition of stream function as the streamlines with $+\Psi$ correspond to anticlockwise circulation, and those with $-\Psi$ correspond to clockwise circulation, respectively. Temperature distribution is also symmetric due to domination of conduction mode of heat transfer. The obtained results are supported by those reported by Sarris et al. [26] but they investigated the case of a square cavity filled with a viscous fluid. Increasing of absolute values of stream function indicates that the flow strength increases with increasing of Rayleigh number and streamlines are more clustered near the top corners. It results in from the increasing of velocity of the fluid flow. As also it is clearly seen from the distribution of the isotherms, these are cumulated around the middle section of the isothermal heater. This result can also be found in Kublbeck et al. [36]. Fig. 5 shows the entropy generation due to fluid flow irreversibility (FFI) (on the left) and heat transfer irreversibility (HTI) (on the right) using the same parameter as in Fig. 4. As it resulted from streamlines and isotherms distributions, the distribution of entropy generation is also symmetric for both FFI and HTI. The entropy generation is concentrated along the heated and cooled part of non-isothermal wall where the temperature gradient has a maximum value. In other words, the actives parts are cumulated on the non-isothermal wall. The reason of this cumulation is that the temperature gradient concentrates along the horizontal wall. The contours of the entropy generation due to HTI moves to the isothermal wall and values of entropy generation due to FFI increases with increasing of Rayleigh number. As Rayleigh number increases, there is a change from conduction dominant region to convection dominant region, respectively.

Fig. 6 displays the streamlines (on the left) and isotherms (on the right) for different inclination angles which changes from $\varphi = 45^\circ$ to $\varphi = 180^\circ$ at $Ra = 500$. The value of $\varphi = 45^\circ$ corresponds to a right-angle triangular enclosure with non-isothermally heated from inclined wall. In this case, two cells were formed in different

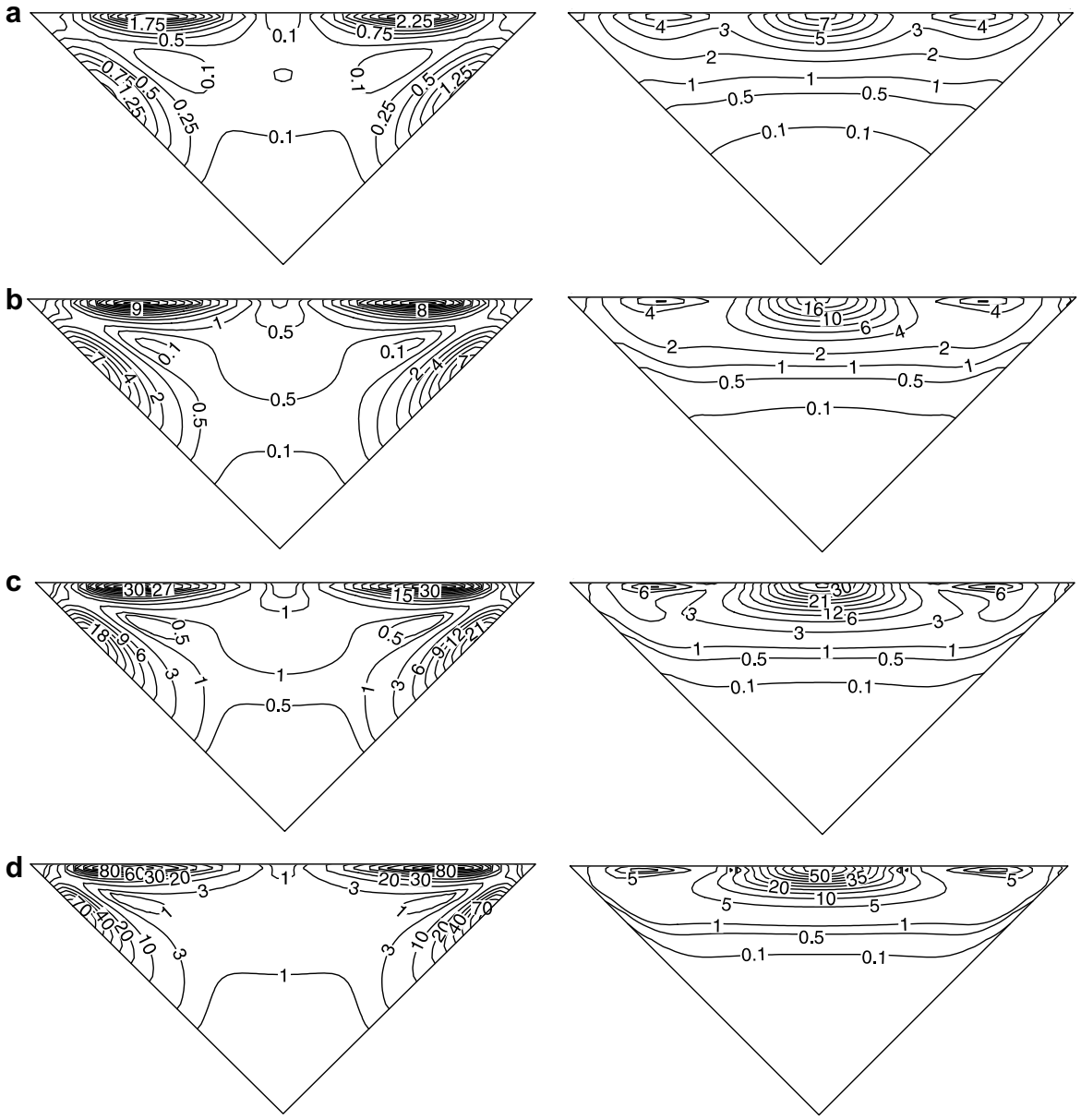

Fig. 5. Entropy generation due to FFI (on the left) and HTI (on the right) for $\varphi = 0^\circ$: (a) $Ra = 100$; (b) $Ra = 250$; (c) $Ra = 500$; (d) $Ra = 1000$.

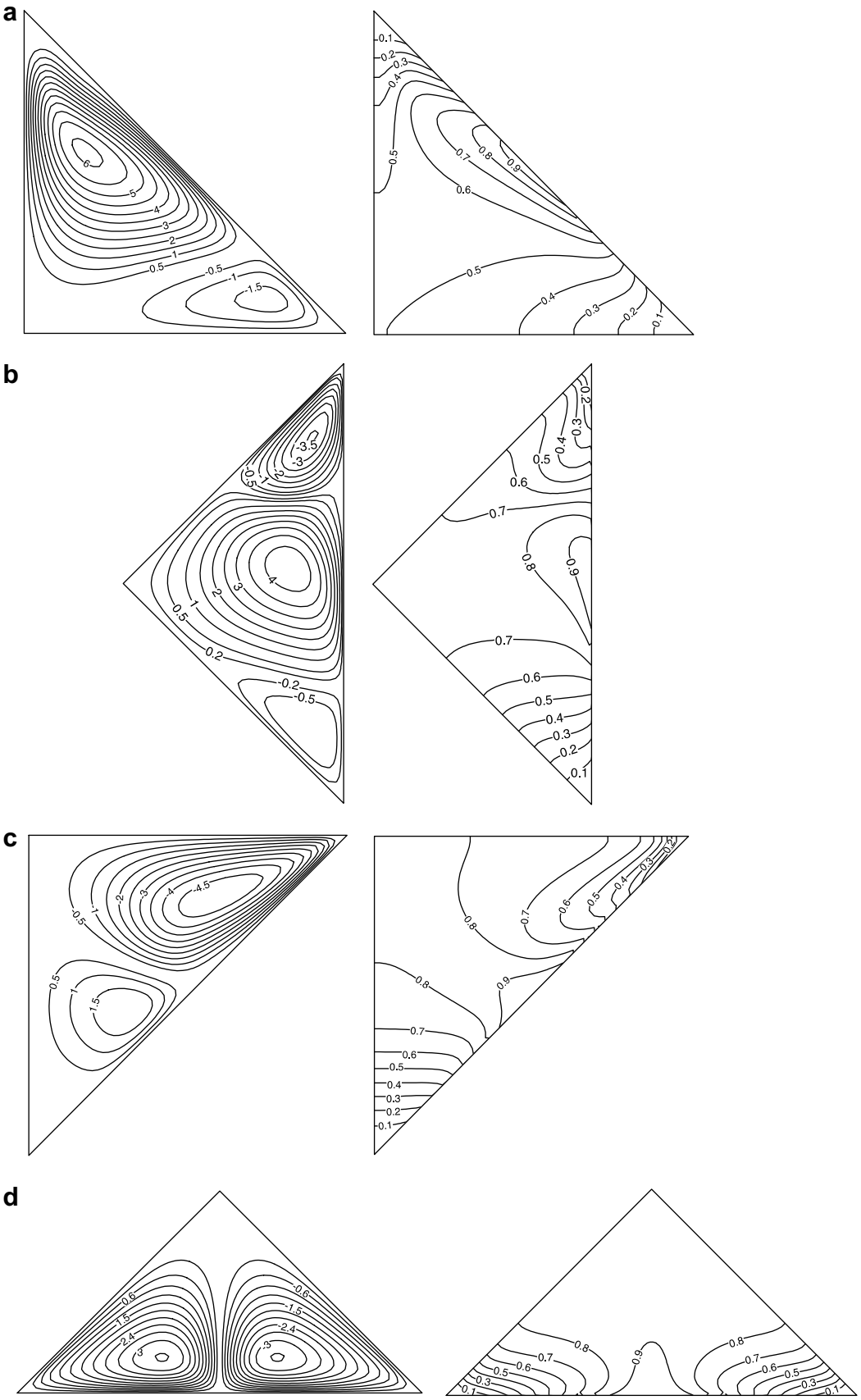

Fig. 6. Streamlines (on the left) and isotherms (on the right) for $Ra = 500$: (a) $\varphi = 45^\circ$; (b) $\varphi = 90^\circ$; (c) $\varphi = 135^\circ$; (d) $\varphi = 180^\circ$.

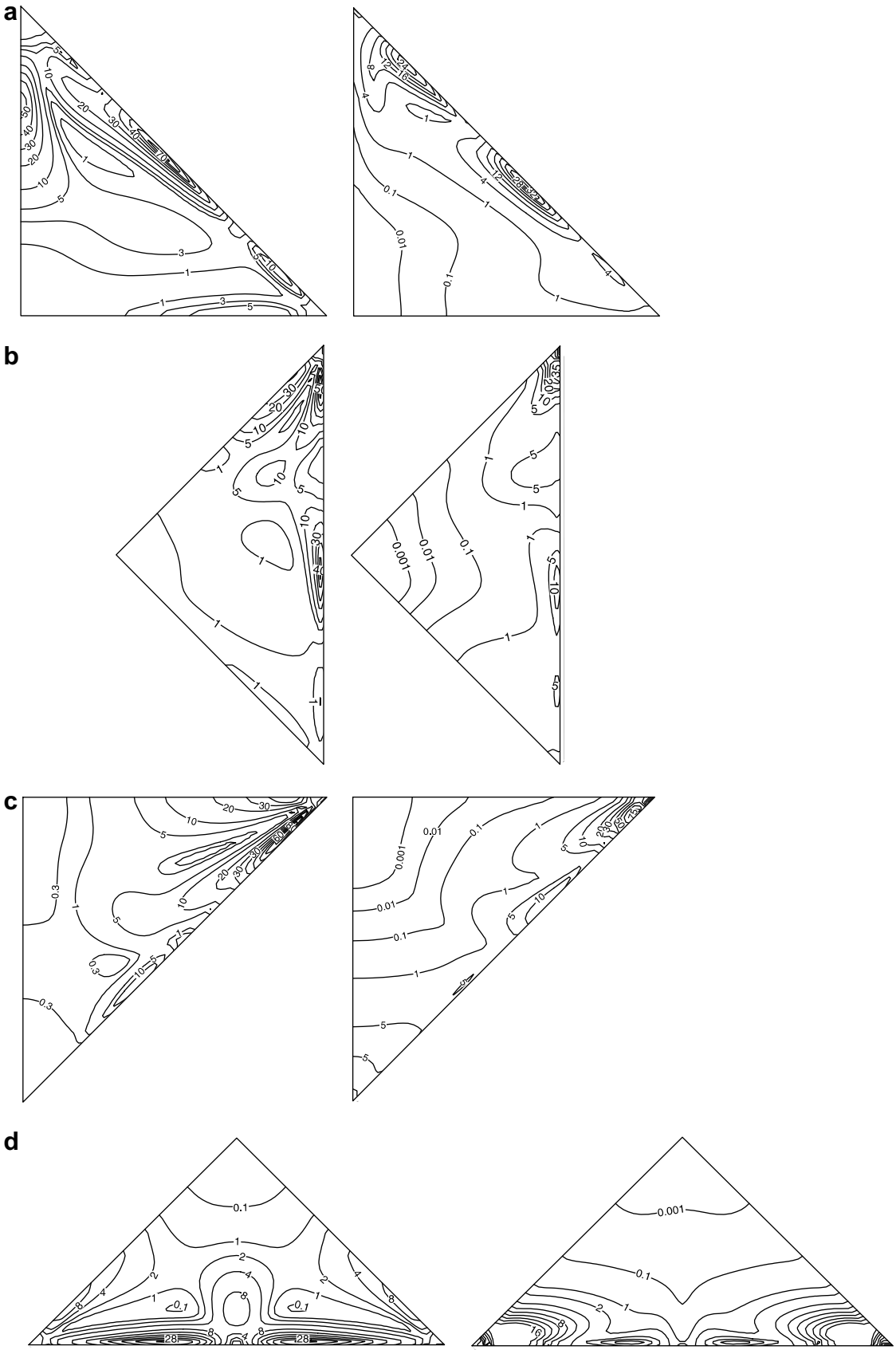

Fig. 7. Entropy generation due to FFI (on the left) and HTI (on the right) for $Ra = 500$: (a) $\varphi = 45^\circ$; (b) $\varphi = 90^\circ$; (c) $\varphi = 135^\circ$); $\varphi = 180^\circ$.

rotating direction as the bottom one clockwise and the top one counter clockwise direction. The fluid, which is near to the hot region of non-isothermal wall, moves upward while the relatively heavy fluid, which is near to cold wall moves downward, and the heated fluid is moving up. Thus, the top cell is dominant at the bottom wall due to moving of hot fluid to the upper top corner. This is also clearly seen from the distribution of the isotherms shown in Fig. 6(a) (on the right). For $\varphi = 90^\circ$, three cells were formed. The bottom and the top ones rotate in clockwise rotating direction and the middle one in counterclockwise. In this position, the heated wall is effective and the main cells are dominant at the bottom and at the top, respectively. There is observed a hill-like temperature distribution or a rain drop-like temperature distribution over the heated region of the cavity and heated fluid moves to the top corner. Isotherms are almost parallel to each other at the bottom corner due to domination of conduction mode of heat transfer (Fig. 6(b)). Looking at the position of $\varphi = 135^\circ$, again two cells were formed and the top one is dominant to the bottom due to increasing of heated part of the fluid. The strength of flow is found to be very weak at the bottom part of the enclosure (Fig. 6(c)). It is interesting to note that, the greater circulation due to position, leads to movement of the elliptical stream function from top right corner to middle of the cavity. Another interesting observation is that the temperature contours are not widely dispersed at the inclined wall. Again, there is a completely symmetric flow and temperature field for the values of inclination angle $\varphi = 180^\circ$ as shown in Fig. 6(d).

Fig. 7(a–d) shows the entropy generation contours (irreversibility maps) due to FFI (on the left) and HTI (on the right) for the same cases with Fig. 6 to see the effects of inclination angle on entropy generation. It can be seen that for $\varphi = 45^\circ$, the entropy generation due to FFI cover whole domain except the left bottom corner of the cavity. The covered domain is affected by changing the inclination angle φ. They are cumulated on three different locations at inclined wall. Active sides are the middle region of the non-isothermal wall for $\varphi = 90^\circ$ and this side changes to right top corner with changing of position from $\varphi = 90^\circ$ to $\varphi = 135^\circ$. This is due to heat transfer irreversibility, since large heat transfer is confined to these locations. Fig. 7(d) shows the symmetric distribution of entropy generation due to symmetric behavior of flow and thermal field as given in Fig. 6(d). As seen from Fig. 7(d) the entropy generation is mostly

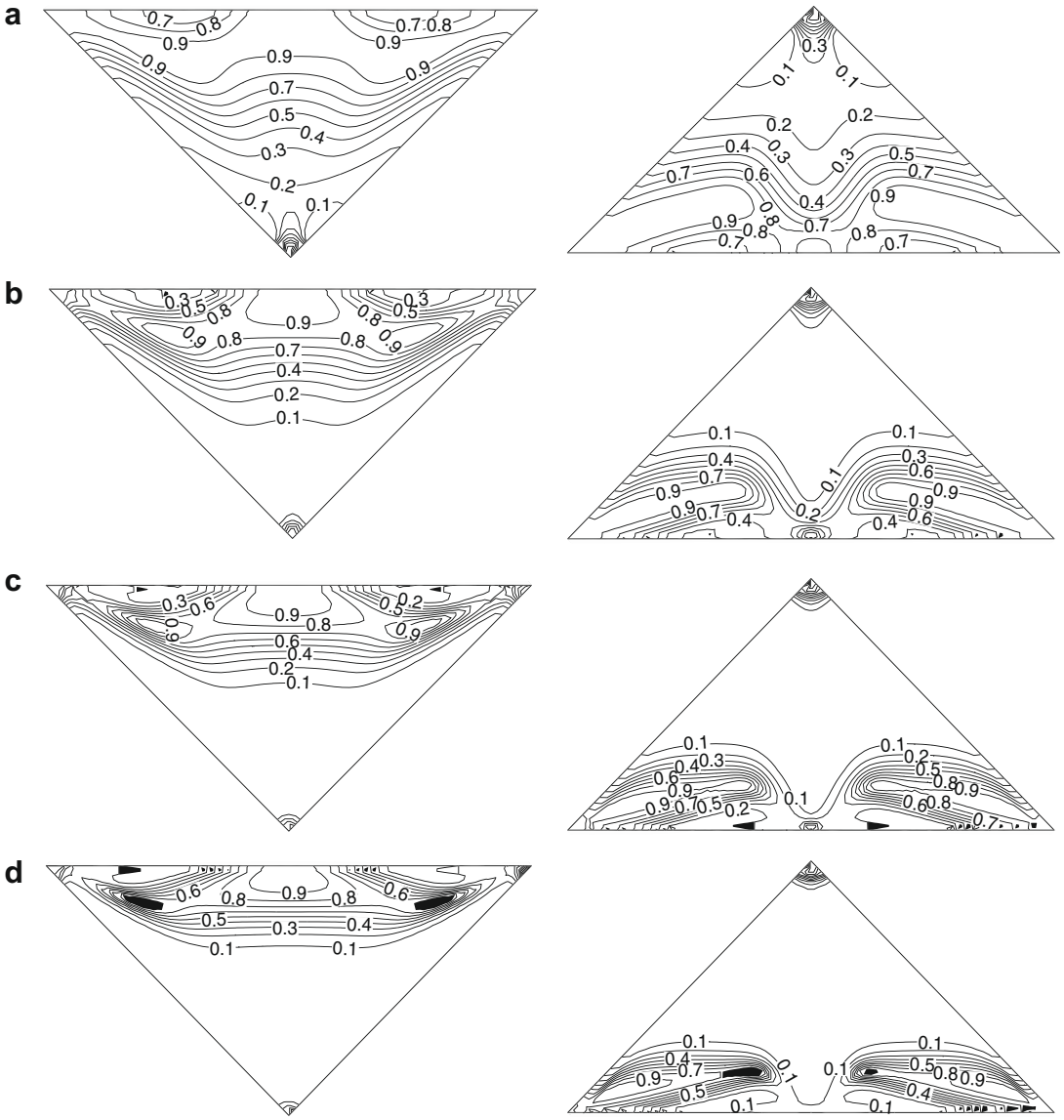

Fig. 8. Iso-Bejan lines at $\varphi = 0^\circ$ (on the left) and $\varphi = 180^\circ$ (on the right): (a) $Ra = 100$; (b) $Ra = 250$; (c) $Ra = 500$; (d) $Ra = 1000$.

localized along the non-isothermal walls. This is due to the boundary layer regime at higher Rayleigh number. This fact is also valid for a rectangular cavity filled with a viscous fluid as studied by Magherbi et al. [37].

The iso-Bejan lines are presented in Fig. 8 for $\varphi = 0^\circ$ (on the left) and $\varphi = 180^\circ$ (on the right), which are opposite cases, at different Rayleigh numbers to see the effects of inclination angle on the ratio between the heat transfer irreversibility and overall entropy generation, which is defined as Bejan numbers. It can be seen that the distribution of iso-Bejan lines are symmetric relative to the bottom corner. Effects of entropy generation due to FFI are higher near the non-isothermal wall but it becomes smaller around the origin. As seen from the streamlines distribution in Fig. 4 (on the left), there is a strong flow friction over the heated region. In this region entropy is generated mostly due to FFI. With the increase of the Rayleigh number, the middle part of the non-isothermal wall becomes effective on entropy generation due to HTI. It is also effective almost on half of the enclosure as given in Fig. 8(b–d). For further values of Rayleigh number, values of iso-Bejan are almost zero. In this case, the entropy generation due to HTI and FFI decreases. It means that there are no irreversibilities at that region and there is no energy loses. For the position of $\varphi = 180^\circ$, a convex shaped distribution is observed for all values of the Rayleigh number. Entropy generation spreads all over the enclosure for low Rayleigh numbers. FFI irreversibility increases with increasing of Rayleigh number and iso-Bejan lines are clustered near the non-isothermal wall of the cavity. At the highest Rayleigh number (Fig. 8(d)), they are cumulated at the corners. Comparison of two position of the enclosure indicates that entropy generation becomes stronger due to FFI in the position of $\varphi = 0^\circ$.

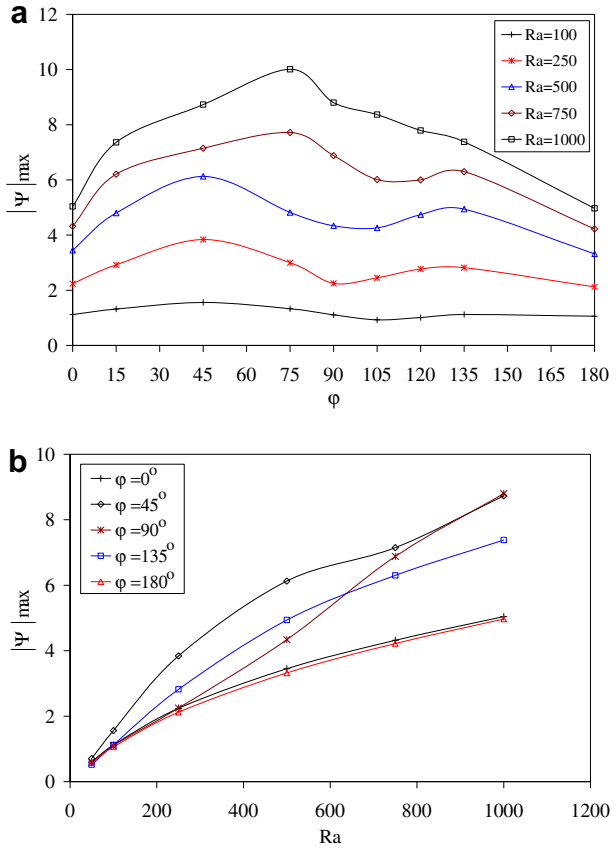

Fig. 9. Variation of the maximum absolute stream function $|\Psi|_{max}$: (a) with the inclination angle φ for different Rayleigh numbers; (b) with the Rayleigh number for different inclination angles.

Fig. 9(a) illustrates the variation of absolute maximum stream function with inclination angle for different Rayleigh numbers. The figure represents a combined measure of intensity and extent of the recirculation region. Values of ϕ are increased up to $\phi = 75^o$ for $Ra = 1000$ and $Ra = 750$, and are also increased up to $\varphi = 45^\circ$ for other values of the Rayleigh number. Then, there is a minimum value between $\varphi = 90^\circ$ for $Ra = 100$, 250 and 500 and $\varphi = 105^\circ$ for $Ra = 750$ and 1000. In the same manner, Fig. 9(b) shows the variation of the absolute maximum stream function with Rayleigh numbers. It is an interesting result that values of stream function increase rapidly for $\varphi = 90^\circ$ due to forming of multiple cells as seen from Fig. 6(b). At this position of the enclosure, a Bénard type cell was formed. Thus, $Ra = 500$ is a critical value for transition of steady-state flow to an unsteady regime for a triangular enclosure at the inclination $\varphi = 90^\circ$. It is noticed that the highest value of the absolute maximum stream function is obtained for $\varphi = 45^\circ$. Another result can be seen from the figure, namely that the stream functions are increased with increasing of Rayleigh numbers. The values are almost equal to each other for $\varphi = 0^\circ$ and $\varphi = 180^\circ$.

Fig. 10(a–e) shows the variation of the local Nusselt number along the heated wall for different Rayleigh numbers and different inclination angles. As it is well-known, higher Rayleigh number means larger heat addition to the system. Namely, intensification of fluid convection increases with increasing of Rayleigh number. Further, Fig. 10 clearly shows that there are positive and negative values of the local Nusselt number. Negative sign means losing heat of the fluid. In the case of $\varphi = 0^\circ$, a symmetric distribution is observed and maximum and minimum values are formed above the center of heated and cooled region at the highest value of Rayleigh number. The similar distribution of local Nusselt number is supported by Sarris et al. [26]. This stems from the symmetric flow pattern as indicated in the above figures. The symmetric distribution becomes distorted for $\varphi = 45^\circ$. Values are almost equal to each other for $X \geqslant 1.1$ on the heated wall. And there is a huge increase of the value of local Nusselt number around $X = 0.22$ due to high circulation intensity. For $\varphi = 90^\circ$, a wavy variation is observed for the local Nusselt number. This is due to presence of the multiple circulation cells as given in Fig. 6(b). Variation of the local Nusselt number along the heated horizontal wall of the cavity is presented in Fig. 10(d) for $\varphi = 135^\circ$. As illustrated in the figure, lower values are formed and these values depend on the position of the enclosure. Again, a symmetric distribution is formed at $\varphi = 180^\circ$. In this case, the flow field also symmetric as given in streamline (on the left) from Fig. 6(d).

Variation of minimum and maximum values of local Nusselt numbers with Rayleigh number is shown in Fig. 11 at different inclination angles. The values are obtained from negative and positive parts of the Nusselt number as illustrated in the small figure at the left side of Fig. 11. These two Nusselt numbers stem from heated and cooled parts of the non-isothermal boundary of the enclosure. Thus, we chose the peak values of both Nusselt numbers for main figure. As given in the figure, the maximum value of the Nusselt number increases monotonically with increasing of Rayleigh number for all values of the inclination angle. The reason of different behavior of Nusselt numbers at $\varphi = 90^\circ$ comes from Rayleigh Bénard like convection as given in Fig. 6(b). As indicated earlier that multiple cells were formed at this value of inclination angle, $\varphi = 90^\circ$. The highest maximum and minimum values are formed for $\varphi = 0^\circ$ and heat transfer decreases for $\varphi = 135^\circ$ and $\varphi = 180^\circ$.

Variation of the Bejan number *Be*, which is calculated using Eq. (9), with the Rayleigh number is given in Fig. 12 for different inclination angles φ. As given in the figure, Bejan number decreases with increasing of Rayleigh number for all values of inclination angle. This is also observed from the work of Magherbi et al. [37]. As it is shown in the literature (Bejan [21], Baytas [23]), $Be = 1.0$ is the

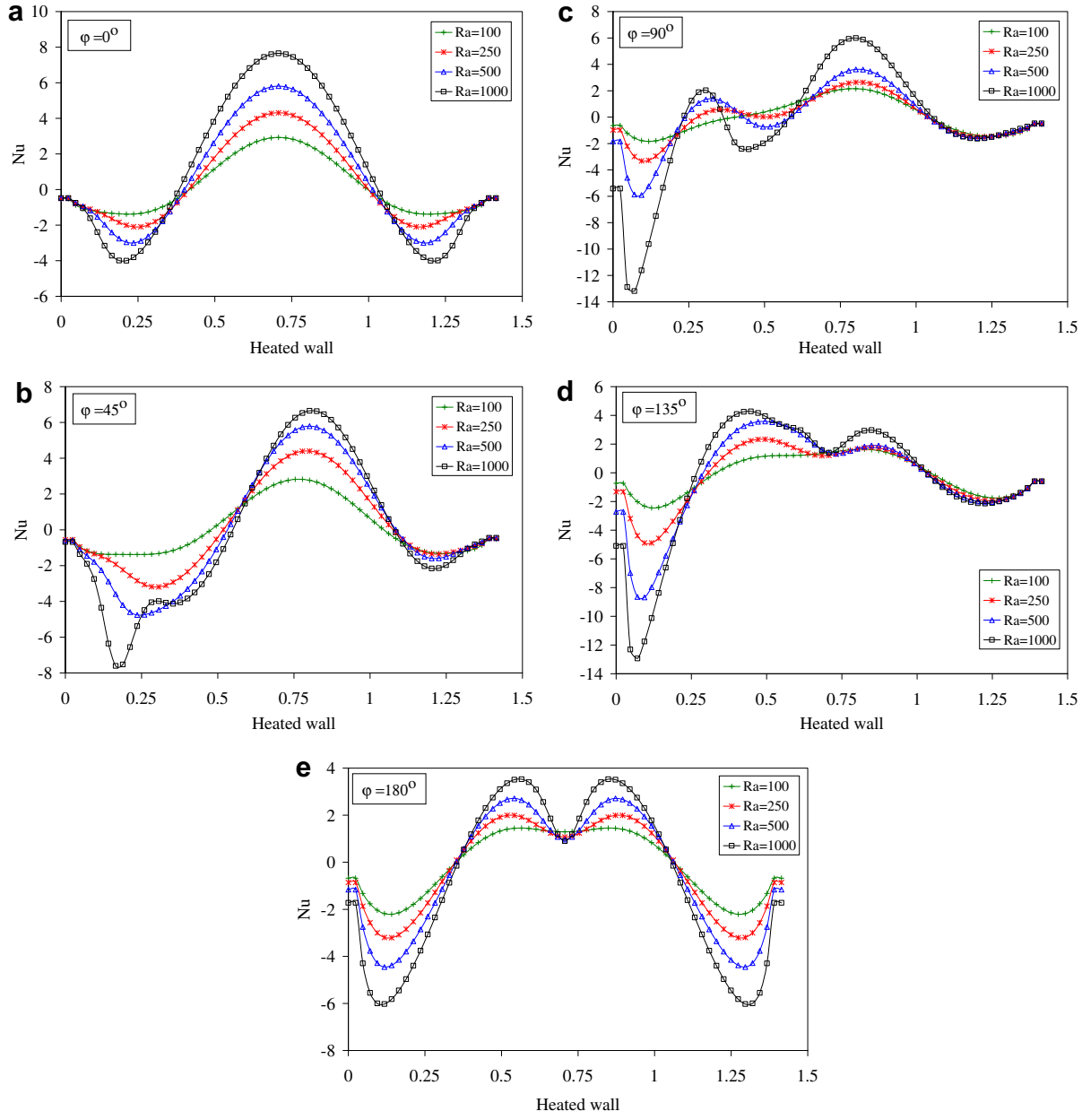

Fig. 10. Variation of local Nusselt number on the heated wall for different Rayleigh numbers: (a) $\varphi = 0^{\circ}$; (b) $\varphi = 45^{\circ}$; (c) $\varphi = 90^{\circ}$; (d) $\varphi = 135^{\circ}$; (e) $\varphi = 180^{\circ}$.

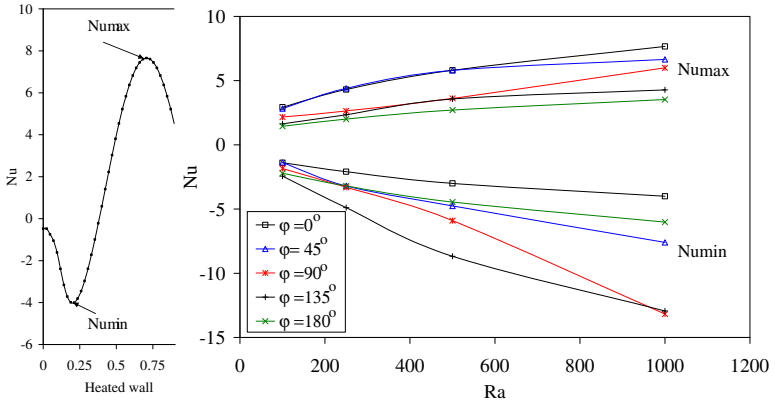

Fig. 11. Variation of maximum and minimum values of Nu on the heated wall with Ra for different inclination angles.

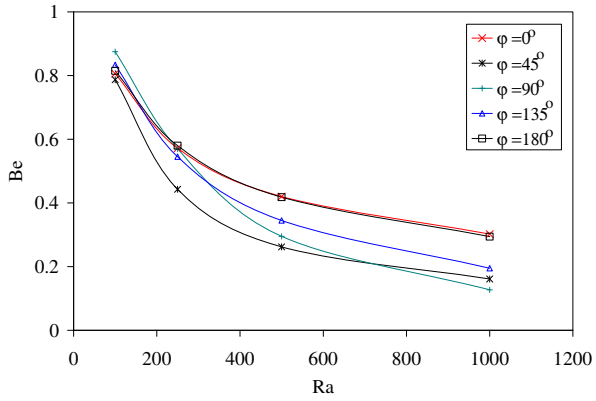

Fig. 12. Variation of Bejan number with Rayleigh number for different inclination angles.

limit at which the irreversibility is due to heat transfer and $Be = 0$ is the irreversibility due to FFI. However, for the case of $Be = 0.5$ entropy generation due to HTI and FFI are equal. For $\varphi = 90^\circ$, HTI irreversibility is dominant for lower Rayleigh number but FFI becomes dominant at $Ra = 1000$. The highest values of Bejan numbers are obtained at the highest Rayleigh number at $\varphi = 0^\circ$. The values are almost equal for $\varphi = 0^\circ$ and $\varphi = 180^\circ$ due to symmetric flow field as indicated in above discussions. Thus, the Bejan number is clearly a measure of the relative magnitude of the entropy generation due to HTI and FFI. As a result, the observations indicate us that the inclination angle φ is a control parameter for entropy generation and saving of energy.

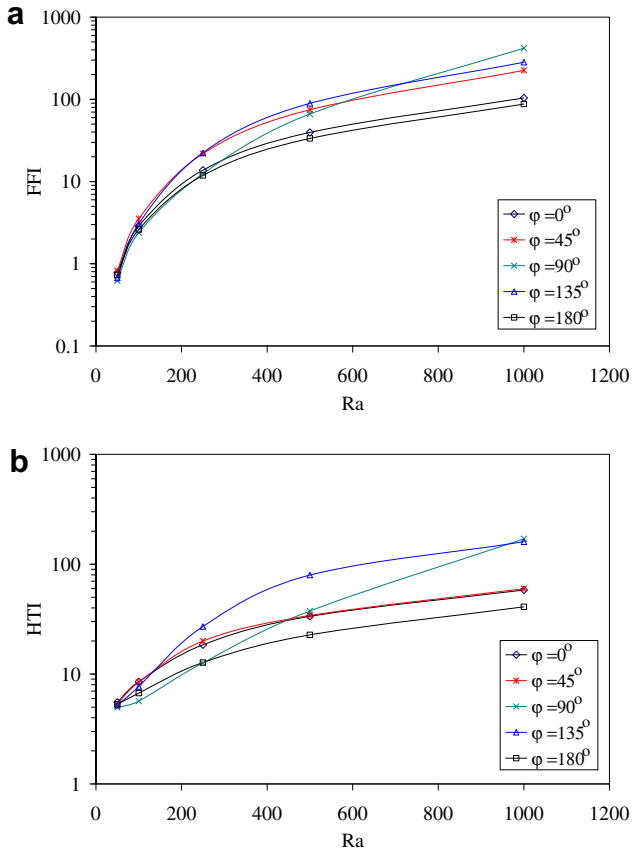

Fig. 13. Variation of entropy generation with Rayleigh number for different inclination angles: (a) FFI; (b) HTI.

Finally, we have presented the variation of entropy generation due to FFI and HTI with Rayleigh number for different inclination angles in Fig. 13(a) and (b). It is seen that the entropy generation increases with increasing of inlet energy to the system, namely increasing of Rayleigh number, which is an expected result, for all inclination angles. This is valid for entropy generation due to both HTI and FFI. At the inclination angle of $\varphi = 180^\circ$, lower values are formed for both HTI and FFI. Entropy generation due to HTI is equal to each other for $\varphi = 45^\circ$ and $\varphi = 180^\circ$. It is an interesting result, that the highest value of entropy generation due to FFI is formed for $\varphi = 90^\circ$. It can be seen from both Figs. 12 and 13 that Rayleigh Bénard convection, which occurs at $\varphi = 90^\circ$, affects the entropy generation for both HTI and FFI.

6. Conclusion

Laminar natural convection and entropy generation in an inclined isosceles triangular enclosure filled with a porous medium has been numerically studied for the case of non-isothermally heated long wall and adiabatic at the equally length walls. Equations of mass, momentum and energy have been written using Darcy law along with the Boussinesq approximation. Isotherms, streamlines, entropy generation due to FFI and HTI, iso-Bejan lines, Nusselt numbers and Bejan numbers have been produced. The influence of inclination angle on the flow patterns and heat transfer characteristics in the enclosure is examined in detail for large range values of the Rayleigh number. It is found that the inclination angle affects the number of cells, circulation intensity and temperature distribution. Thus, heat transfer and circulation intensity decrease when non-isothermal wall locates at the top. A symmetric flow and temperature distribution is observed for $\varphi = 180^\circ$ and $\varphi = 0^\circ$, and the Bejan numbers are equal for these inclination angles. The highest entropy generation due to HTI and FFI and stream function are observed at $\varphi = 90^\circ$ and multiple cells were formed at this angle. Both entropy generation and heat transfer increase with increasing of Rayleigh number. Flow strength also increases and isotherms are clustered near non-isothermal wall with Rayleigh number. Bejan number is decreased with entropy generation and FFI becomes dominant near the non-isothermal wall especially at high Rayleigh numbers. Heat losses are increased with increasing of inclination angle and local Nusselt numbers are symmetric for $\varphi = 180^\circ$ and $\varphi = 0^\circ$.

Acknowledgements

The authors express their thanks to the reviewers for the valuable comments and suggestions.

References

[1] P. Cheng, Heat transfer in geothermal systems, Adv. Heat Transfer 14 (1979) 1–105.
[2] A. Bejan, Convective heat transfer in porous media, in: S. Kakaç, R.K. Shah, W. Aung (Eds.), Handbook of Single-Phase Convective Heat Transfer, Wiley, New York, 1987.
[3] D.A. Nield, A. Bejan, Convection in Porous Media, third ed., Springer, New York, 2006.
[4] D.B. Ingham, A. Bejan, E. Mamut, I. Pop, Emerging Technologies and Techniques in Porous Media, Kluwer, Dordrecht, 2004.
[5] D.B. Ingham, I. Pop (Eds.), Transport Phenomena in Porous Media, Elsevier, Oxford, 2005 (vol. III).
[6] K. Vafai (Ed.), Handbook of Porous Media, second ed., Taylor & Francis, New York, 2005.
[7] P. Vadasz (Ed.), Emerging Topics in Heat and Mass Transfer in Porous Media, Springer, New York, 2008.
[8] A. Bejan, D. Poulikakos, Natural convection in an attic-shaped space filled with porous material, J. Heat Transfer 104 (1982) 241–247.
[9] V.A. Akinsete, T.A. Coleman, Heat transfer by steady laminar free convection in triangular enclosures, Int. J. Heat Mass Transfer 25 (1982) 991–998.

[10] H. Asan, L. Namli, Laminar natural convection in a pitched roof of triangular cross-section: summer day boundary conditions, Energy Buildings 33 (2000) 69–73.
[11] H. Asan, L. Namli, Numerical simulation of buoyant flow in a roof of triangular cross section under winter day boundary conditions, Energy Buildings 33 (2001) 753–757.
[12] E.H. Ridouane, A. Campo, M. Hasnaoui, Benefits derivable from connecting the bottom and top walls of attic enclosures with insulated vertical side walls, Numer. Heat Transfer Part A 49 (2006) 175–193.
[13] G.A. Holtzman, R.W. Hill, K.S. Ball, Laminar natural convection in isosceles triangular enclosures heated from below and symmetrically cooled from above, J. Heat Transfer 122 (2000) 485–491.
[14] T. Basak, S. Roy, S. Krishna Babu, A.R. Balakrishnan, Finite element analysis of natural convection flow in a isosceles triangular enclosure due to uniform and non-uniform heating at the side walls, Int. J. Heat Mass Transfer 51 (2008) 4496–4505.
[15] T. Basak, S. Roy, S. Krishna Babu, I. Pop, Finite element simulations of natural convection flow in an isosceles triangular enclosure filled with a porous medium: effects of various thermal boundary conditions, Int. J. Heat Mass Transfer 51 (2008) 2733–2741.
[16] Y. Varol, H.F. Oztop, A. Varol, Free convection in porous media filled right-angle triangular enclosures, Int. Commun. Heat Mass Transfer 33 (2006) 1190–1197.
[17] Y. Varol, H.F. Oztop, A. Varol, Natural convection in porous triangular enclosures with a solid adiabatic fin attached to the horizontal wall, Int. Commun. Heat Mass Transfer 34 (2007) 19–27.
[18] Y. Varol, H.F. Oztop, T. Yilmaz, Two-dimensional natural convection in a porous triangular enclosure with a square body, Int. Commun. Heat Mass Transfer 34 (2007) 238–247.
[19] T. Basak, S. Roy, C. Thirumalesha, Finite element simulations of natural convection in a right-angle triangular enclosure filled with a porous medium: effects of various thermal boundary conditions, J. Porous Media 11 (2008) 159–178.
[20] T. Basak, S. Roy, S. Krishna Babu, Natural convection and flow simulation in differentially heated isosceles triangular enclosures filled with porous medium, Chem. Eng. 63 (2008) 3328–3340.
[21] A. Bejan, Entropy Generation through Heat and Fluid Flow, John Wiley & Sons, 1994.
[22] A. Bejan, Entropy Generation Minimization, CRC, 1995.
[23] A.C. Baytas, Entropy generation for natural convection in an inclined porous cavity, Int. J. Heat Mass Transfer 43 (2000) 2089–2099.
[24] I. Zahmatkesh, On the importance of thermal boundary conditions in heat transfer and entropy generation for natural convection inside a porous enclosure, Int. J. Therm. Sci. 47 (2008) 339–346.
[25] Y. Varol, H.F. Oztop, A. Koca, Entropy production due to free convection in partially heated isosceles triangular enclosures, Appl. Therm. Eng. 28 (2008) 1502–1513.
[26] I.E. Sarris, I. Lekakis, N.S. Vlachos, Natural convection in a 2D enclosure with sinusoidal upper wall temperature, Numer. Heat Transfer Part A 42 (2002) 513–530.
[27] E. Bilgen, R. Ben-Yedder, Natural convection in enclosure with heating and cooling by sinusoidal temperature profiles on one side, Int. J. Heat Mass Transfer 50 (2007) 139–150.
[28] N.H. Saeid, Natural convection in porous cavity with sinusoidal bottom wall temperature variation, Int. Commun. Heat Mass Transfer 32 (2005) 454–463.
[29] Y. Varol, H.F. Oztop, I. Pop, Numerical analysis of natural convection for a porous rectangular enclosure with sinusoidally varying temperature profile on the bottom wall, Int. Commun. Heat Mass Transfer 35 (2008) 56–64.
[30] B. Alazmi, K. Vafai, Constant wall heat flux boundary conditions in porous media under local thermal non-equilibrium conditions, Int. J. Heat Mass Transfer 45 (2002) 3071–3087.
[31] R.J. Gross, M.R. Bear, C.E. Hickox, The application of flux-corrected transport (FCT) to high Rayleigh number natural convection in a porous medium, Proc. 8th Int. Heat Transfer Conf., San Francisco, CA, 1986.
[32] B. Goyeau, J.P. Songbe, D. Gobin, Numerical study of double-diffusive natural convection in a porous cavity using the Darcy–Brinkman formulation, Int. J. Heat Mass Transfer 39 (1996) 1363–1378.
[33] D.M. Manole, J.L. Lage, Numerical benchmark results for natural convection in a porous medium cavity, Heat and Mass Transfer in Porous Media, ASME Conf., HTD-216 (1992) 55–60.
[34] N.H. Saeid, I. Pop, Natural convection from a discrete heater in a square cavity filled with a porous medium, J. Porous Media 8 (2005) 55–63.
[35] A.C. Baytas, I. Pop, Free convection in a square porous cavity using a thermal nonequilibrium model, Int. J. Therm. Sci. 41 (2002) 861–870.
[36] K. Kublbeck, G.P. Merker, J. Straub, Advanced numerical computation of two-dimensional time-dependent free convection in cavities, Int. J. Heat Mass Transfer 23 (1980) 203–217.
[37] M. Magherbi, H. Abbassi, A. Ben Ibrahim, Entropy generation at the onset of natural convection, Int. J. Heat Mass Transfer 46 (2003) 3441–3450.